

A Search for various Double Beta Decay Modes of Cd, Te and Zn Isotopes

H. Kiel, D. Münstermann

*Lehrstuhl für Experimentelle Physik IV, Universität Dortmund,
Otto-Hahn Str. 4, 44221 Dortmund, Germany*

K. Zuber

*Denys Wilkinson Laboratory, Dept. of Physics, University of Oxford,
Keble Road, Oxford, OX1 3RH, UK*

Abstract

Various double beta decay modes of Cd, Zn and Te isotopes are explored with the help of CdTe and CdZnTe semiconductor detectors. The data set is splitted in an energy range below 1 MeV having a statistics of 134.5 g·d and one above 1 MeV resulting in 532 g·d. No signals were observed in all channels under investigation. New improved limits for the neutrinoless double beta decay of ^{70}Zn of $T_{1/2} > 1.3 \cdot 10^{16} \text{ yrs}$ (90% CL), the longest standing limit of all double beta isotopes, and $0\nu\beta^+\text{EC}$ of ^{120}Te of $T_{1/2} > 2.2 \cdot 10^{16} \text{ yrs}$ (90% CL) are given. For the first time a limit on the half-life of the $2\nu\text{ECEC}$ of ^{120}Te of $T_{1/2} > 9.4 \cdot 10^{15} \text{ yrs}$ (90% CL) is obtained. In addition, limits on $2\nu\text{ECEC}$ for ground state transitions of ^{106}Cd , ^{108}Cd and ^{64}Zn are improved. The obtained results even under rough background conditions show the reliability of CdTe semiconductor detectors for rare nuclear decay searches.

Key words: Neutrino mass, double beta decay, lepton number violation

PACS: 23.40.-s, 21.10.Tg, 27.60.+j, 29.40.Wk

1 Introduction

Conservation laws play a crucial role in modern particle physics, normally resulting from invariances under certain symmetry transformations. However, there are symmetries in the Standard Model, where such an underlying invariance is not known, the most popular ones are baryon and lepton number conservation. Therefore, the investigation of lepton number violating processes is one of the most promising ways of probing physics beyond the Standard

Model. A particular aspect of this topic is lepton number violation in the neutrino sector, which in the case of massive neutrinos would allow a variety of new phenomena, for a recent review see [1].

Lepton number violation emerges immediately in case of the existence of Majorana masses of the neutrino, which is predicted in most GUT-theories, by using the see-saw mechanism to explain small neutrino masses [2,3,4].

The gold-plated channel to probe the Majorana character of neutrinos is the $\Delta L = 2$ process of neutrinoless double beta decay ($0\nu\beta^-\beta^-$):

$$(Z, A) \rightarrow (Z + 2, A) + 2e^- \quad (1)$$

The measured half-life is correlated with the neutrino mass via

$$T_{1/2}^{-1} = G^{0\nu} M_{0\nu}^2 \left(\frac{\langle m_{ee} \rangle}{m_e} \right)^2 \quad (2)$$

with $G^{0\nu}$ as the phase space and $M_{0\nu}^2$ as the nuclear transition matrix elements. The quantity $\langle m_{ee} \rangle$ is called the effective Majorana mass and is given by

$$\langle m_{ee} \rangle = \left| \sum U_{ei}^2 m_i \eta^{CP} \right| \quad (3)$$

where m_i are the mass eigenstates, $\eta^{CP} = \pm 1$ the relative CP-phases and U_{ei} the mixing matrix elements. The other eight possible effective Majorana masses $\langle m_{\alpha\beta} \rangle$ with $\alpha, \beta = e, \mu, \tau$ are currently not restricted at all [5].

In addition, the Standard Model process of $2\nu\beta\beta$ -decay can occur

$$(Z, A) \rightarrow (Z + 2, A) + 2e^- + 2\bar{\nu}_e \quad (4)$$

whose detection is important to check the reliability of nuclear matrix element calculations. Various other mechanisms beside a light Majorana neutrino exchange have been proposed to mediate $0\nu\beta\beta$ -decay, among them are e.g. right-handed weak currents [6] and R-parity violating SUSY [7,8]. To disentangle the underlying mechanism it is worthwhile to explore additional processes. In case of the existence of right handed weak currents the full Hamiltonian for double beta decay can be written as

$$H \sim (j_L J_L^\dagger + \kappa j_L J_R^\dagger + \eta j_R J_L^\dagger + \lambda j_R J_R^\dagger) \quad (5)$$

where j denoting leptonic currents and J hadronic currents and $\kappa, \eta, \lambda \ll 1$. The subscript L denotes left-handed weak charged currents of (V-A) structure

and R corresponds to right-handed weak charged currents of (V+A) type, which have not been observed yet. In this case eq. 2 has to be replaced by

$$T_{1/2}^{-1} = C_{mm} \left(\frac{\langle m_{\nu_e} \rangle}{m_e} \right)^2 + C_{\eta\eta} \langle \eta \rangle^2 + C_{\lambda\lambda} \langle \lambda \rangle^2 \quad (6)$$

$$+ C_{m\eta} \left(\frac{\langle m_{\nu_e} \rangle}{m_e} \right) \langle \eta \rangle + C_{m\lambda} \left(\frac{\langle m_{\nu_e} \rangle}{m_e} \right) \langle \lambda \rangle + C_{\eta\lambda} \langle \eta \rangle \langle \lambda \rangle \quad (7)$$

where the coefficients C contain the phase space factors and the matrix elements and

$$\langle \eta \rangle = \eta \sum_j U_{ej} V_{ej} \quad \langle \lambda \rangle = \lambda \sum_j U_{ej} V_{ej} \quad (8)$$

V_{ej} correspond to the mixing matrix elements among the right-handed neutrino states. This results in an ellipsoid in the three parameters $\langle m_{\nu_e} \rangle$, $\langle \lambda \rangle$ and $\langle \eta \rangle$. Decay modes which are dominantly driven by right-handed weak currents are transitions to excited states and $\beta^+ \beta^+$ -decays. The latter can occur in three variants:

$$(Z, A) \rightarrow (Z - 2, A) + 2e^+ (+2\nu_e) \quad (\beta^+ \beta^+) \quad (9)$$

$$e_B^- + (Z, A) \rightarrow (Z - 2, A) + e^+ (+2\nu_e) \quad (\beta^+ / \text{EC}) \quad (10)$$

$$2e_B^- + (Z, A) \rightarrow (Z - 2, A) (+2\nu_e) \quad (\text{EC} / \text{EC}) \quad (11)$$

Like in $0\nu\beta^-\beta^-$ the processes (9)-(11) can occur with and without the emission of neutrinos. The Q-value of the transition is reduced by $m_e c^2$ for any produced positrons. Therefore, EC/EC has the largest phase space. Clearly neutrinoless EC/EC in the stated form violates energy and momentum conservation, therefore additional particles have to be emitted. As discussed in [9] the most likely mechanism is the creation of an additional electron-positron pair via internal conversion. How both modes might disentangle the underlying parameters is shown in figure 1 following the description of [10].

In this paper we explore the various decay channels of Cd, Te and Zn isotopes. This is done by using CdZnTe and CdTe semiconductor detectors as a first step towards the realisation of the COBRA-project [13]. The corresponding decay schemes of all investigated isotopes are shown in figure 2, taken from [14]. For a recent review on double beta decay see [15] and a compilation of current results can be found in [16,17].

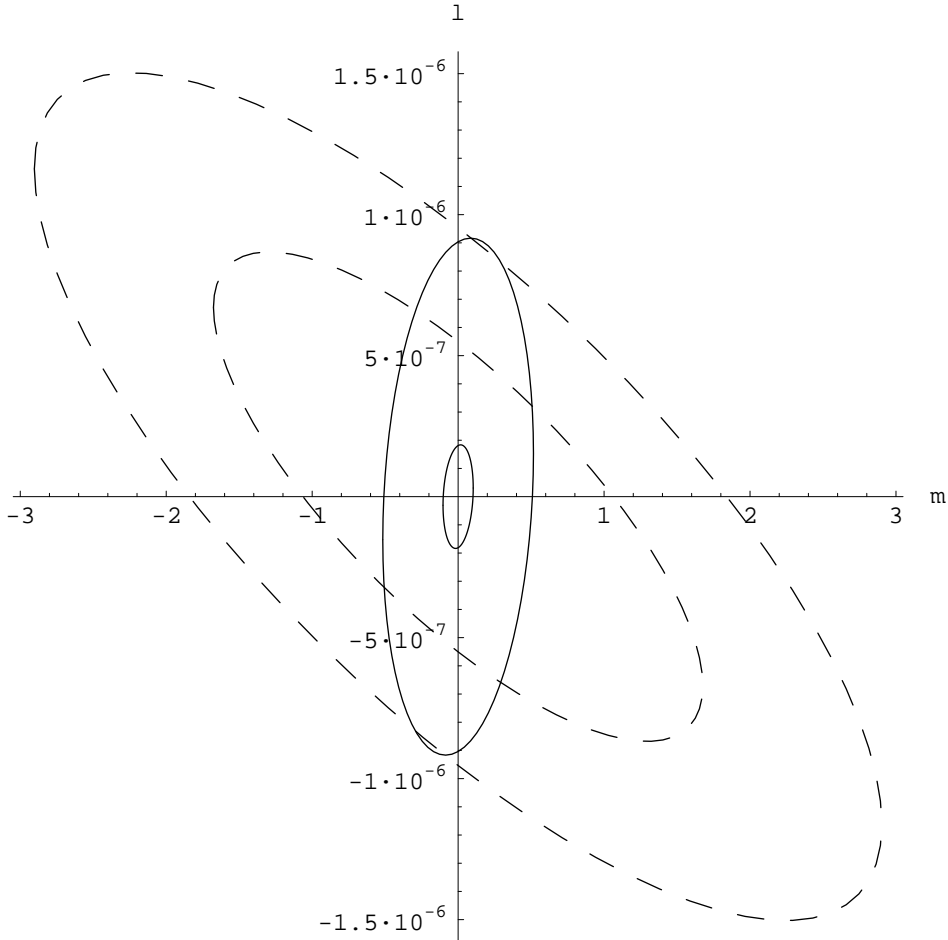


Fig. 1. Complementary of $0\nu\beta\beta$ -decay and $\beta^+\beta^+$ -decay modes. Shown is the $\langle \lambda \rangle - \langle m_{\nu_e} \rangle$ plane (assuming $\langle \eta \rangle = 0$ for simplicity). The small ellipse (solid line) corresponds to the allowed parameter values of the recently claimed evidence for $0\nu\beta\beta$ -decay [11] (see also [12]). Also shown are the parameter regions (dashed lines) corresponding to a possible $\beta^+\beta^+$ -measurement with a half-life between $1 \cdot 10^{26}$ and $3 \cdot 10^{26}$ years.

2 Experimental setup

This analysis is based on measurements performed with two detectors, a 2.89 g $10 \times 10 \times 5 \text{ mm}^3$ CdZnTe detector provided by eV-PRODUCTS and a 5.8 g $10 \times 10 \times 10 \text{ mm}^3$ CdTe detector purchased from EURORAD. Both are standard industrial products. The first detector (CPG) and its preamplifier are encapsulated within an aluminium tube with a 2 cm tungsten shield in between. The second detector (ER) is situated in a copper case with the preamplifier outside of a passive shielding.

The ER detector is read out conventionally and shows asymmetric photo peaks with a typical tail towards lower energies due to insufficient collection of pro-

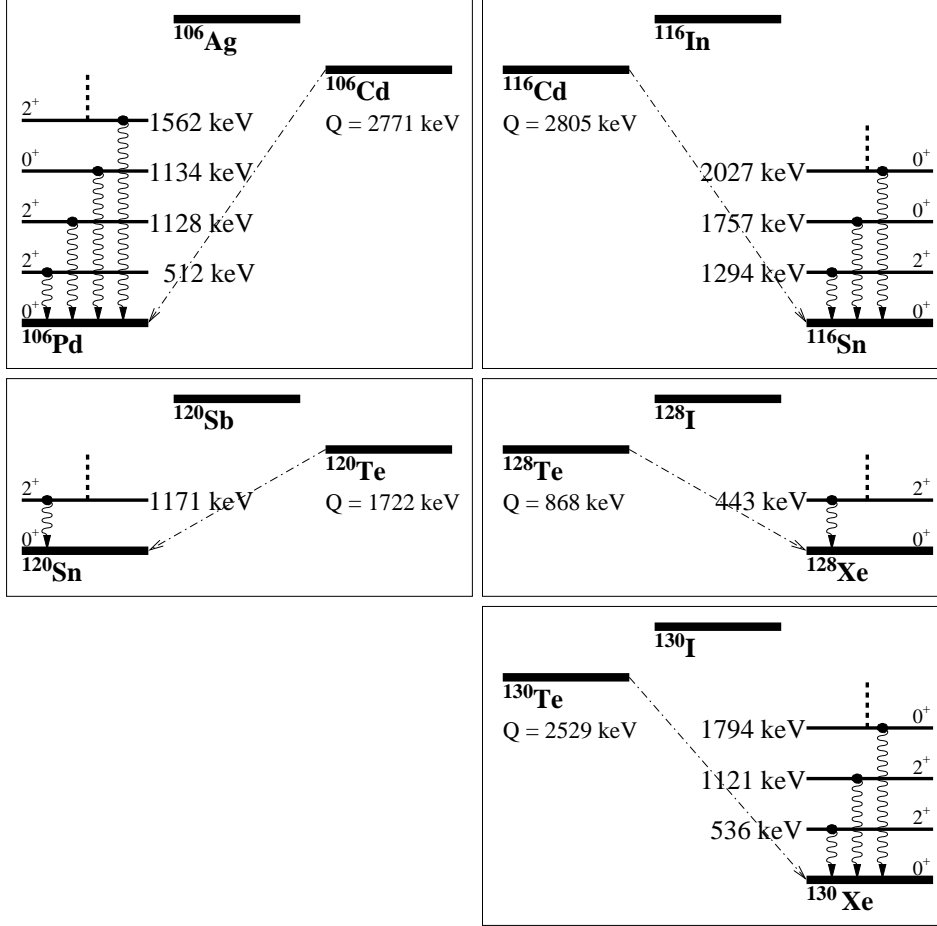


Fig. 2. Decay schemes of the various double beta transitions to excited states. The energies of all investigated $J^\pi = 0^+$ and 2^+ states are given with their respective energy levels. Left: $\beta^+\beta^+$ -decay, right: $\beta^-\beta^-$ -decay. Top: ^{106}Cd and ^{116}Cd , middle: ^{120}Te and ^{128}Te , bottom: ^{130}Te .

duced holes caused by trapping, whereas for the CPG detector the readout is based on coplanar grid technology. This technique allows to read out the pure electron signal only resulting in almost symmetric photo peaks [18].

To explore decays with extremely low expected decay rates, certain prerequisites have to be taken to reduce the background to a minimum. To achieve this, a special shielding (figure 3) has been set up to reduce background coming from cosmic ray muons and environmental radioactivity. This shielding consists of passive and active components. The passive part is a $50 \times 50 \times 50 \text{ cm}^3$ casing made of copper and lead where the inner layer around the detectors consists of electrolytic copper and the outer layer of spectroscopy lead. The lead bricks have been cleaned in an ultrasonic acetone bath and their surfaces have been etched with HCl and HNO_3 before assembly. This 1.4 t passive shielding is covered with an airtight $60 \times 60 \times 60 \text{ cm}^3$ aluminium box constantly flushed with nitrogen to protect the apparatus from ^{222}Rn . The detectors themselves

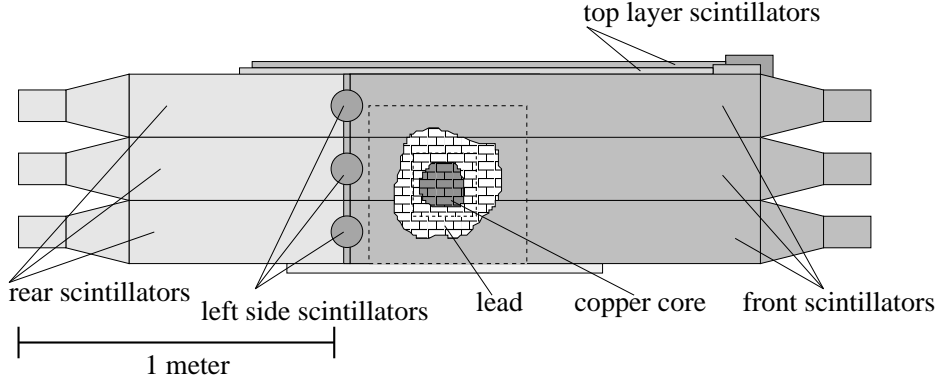


Fig. 3. Schematic drawing of the used setup showing the active and passive shielding components.

are located in a specially manufactured copper brick.

The active part of the shielding against cosmic rays consists of 19 plastic scintillators of $130 \times 20 \times 0.5 \text{ cm}^3$ mounted on the aluminium box. The four sides are covered with one layer of three scintillators each and the top with two layers of four and three scintillators displaced by 50% of their width to minimize dead areas. All photomultiplier signals are fed into discriminators whose OR output signal triggers a $20 \mu\text{s}$ long veto. Running at a trigger rate of about 800 Hz the resulting dead time is 1.65%. The detection efficiency of cosmic ray muons is 95% for a single layer and about 99.7% for the double layer.

The whole apparatus is located in a building with barite concrete walls and ceilings resulting in a total shielding of about 5 mwe.

The data acquisition is done with a 13bit PC multichannel analyser (MCA). The pre-amplified signals of the detectors are fed into shaping amplifiers with a shaping time of $0.5 \mu\text{s}$. The gain of the amplifiers is adjusted to produce a signal of approximately 10 V at 4 MeV, which is the maximal allowed input voltage of the MCA's ADC. The lower threshold is chosen such that the dead time of the ADC did not exceed 2%.

The energy resolution of the detectors was measured with various sources, among them ^{241}Am , ^{57}Co , ^{137}Cs , ^{60}Co and ^{228}Th (figure 4) and is assumed to rise with the square root of the energy within the region of interest. The resulting FWHM energy resolution for the CPG detector is $\Delta E_{\text{CPG}} = \sqrt{E/\text{keV}} \times 1.03 \text{ keV} - 0.72 \text{ keV}$ and for the ER detector $\Delta E_{\text{ER}} = \sqrt{E/\text{keV}} \times 1.68 \text{ keV} + 3.66 \text{ keV}$. The sources were also used for regular calibrations during data taking to assure stable operation of the detectors. Hence, it could be shown that the variation of the peak positions is well below 0.5 %.

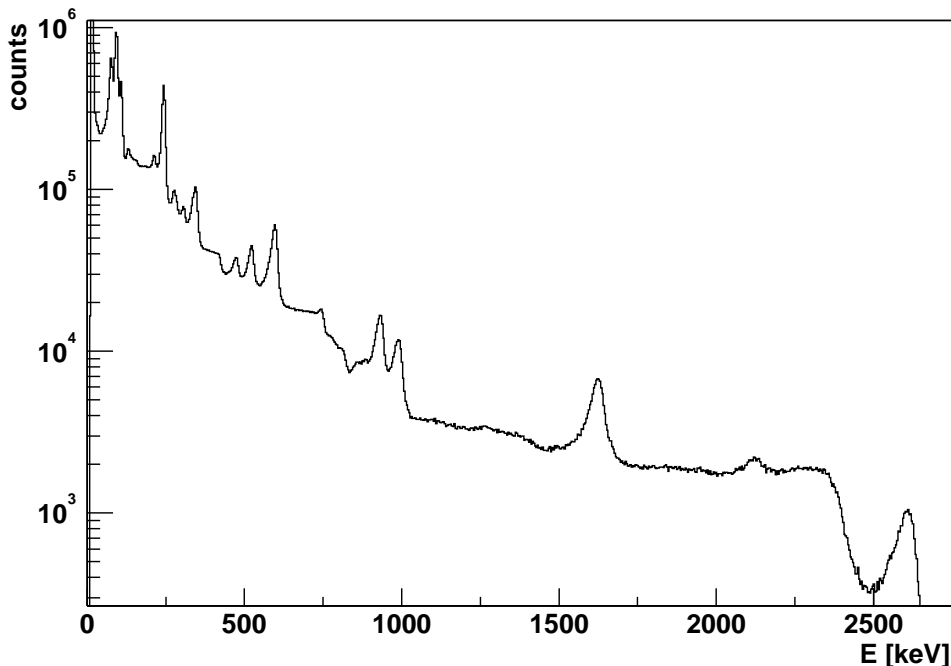


Fig. 4. ^{228}Th spectrum as obtained with the CPG detector. The most prominent lines at 238.6 keV, 583.19 keV, 911.21 keV, 968.97 keV, 1592 keV and 2614 keV are clearly visible. The ^{208}Tl line at 2614 keV serves as an important calibration point because of its close location to the $0\nu\beta\beta$ -decay regions of the ^{116}Cd and ^{130}Te decays.

3 Data Reduction

During the data taking phase runs of 30 minutes life-time have been recorded. The distribution of obtained single runs follows nicely a Poisson distribution, however, there are a few bursts, probably due to electric disturbances. Such runs were discarded, in case of the CPG detector there were two such burst runs. The remaining runs show a stable event rate for the intervals 150 keV - 300 keV and 0.5 MeV - 2 MeV (figure 5) leading to a total measuring time of 1117 hours. The rebinned final spectrum used for the analysis is shown in figure 6.

The spectrum shows several features of background sources. The most prominent signature is a bump below 300 keV which can be attributed to the four-fold forbidden non-unique beta spectrum of ^{113}Cd . Also visible are small peaks of the ^{238}U (351 keV and 609 keV) and ^{232}Th (238.6 keV and 338 keV) decay chains.

For the ER detector also runs of 30 minutes length have been recorded. However, in these runs some systematic irregularities are apparent in the low energy range. Therefore, below 1 MeV a variation in the average rates could be observed, making the data unreliable in that region. For the spectrum above

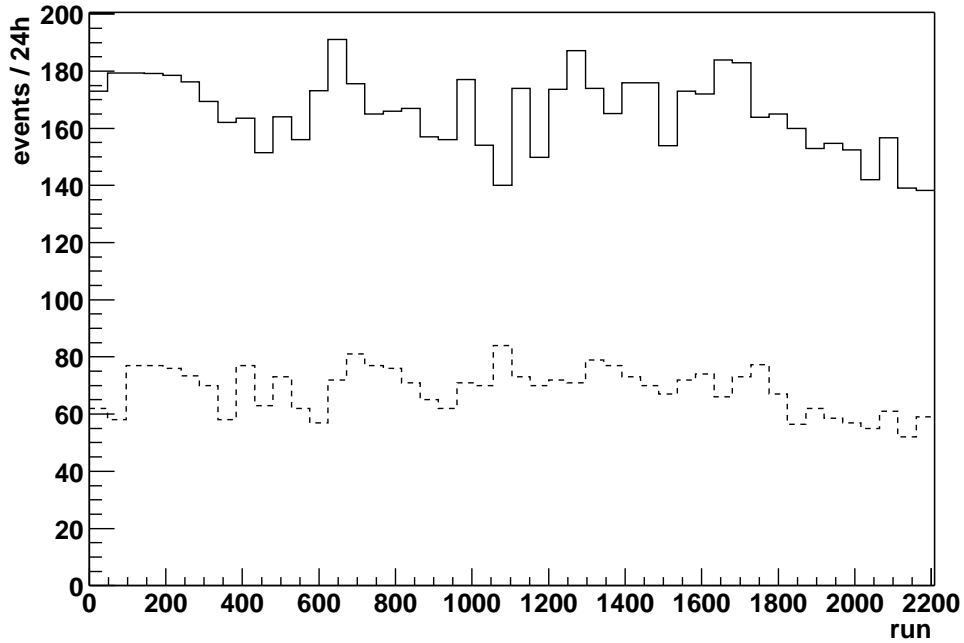


Fig. 5. Events per day for recorded CPG data in the intervals 150-300 keV (solid line), 0.5-2 MeV (dashed line), confirming stable operation of the detector. The run period shown corresponds to about 46.5 days.

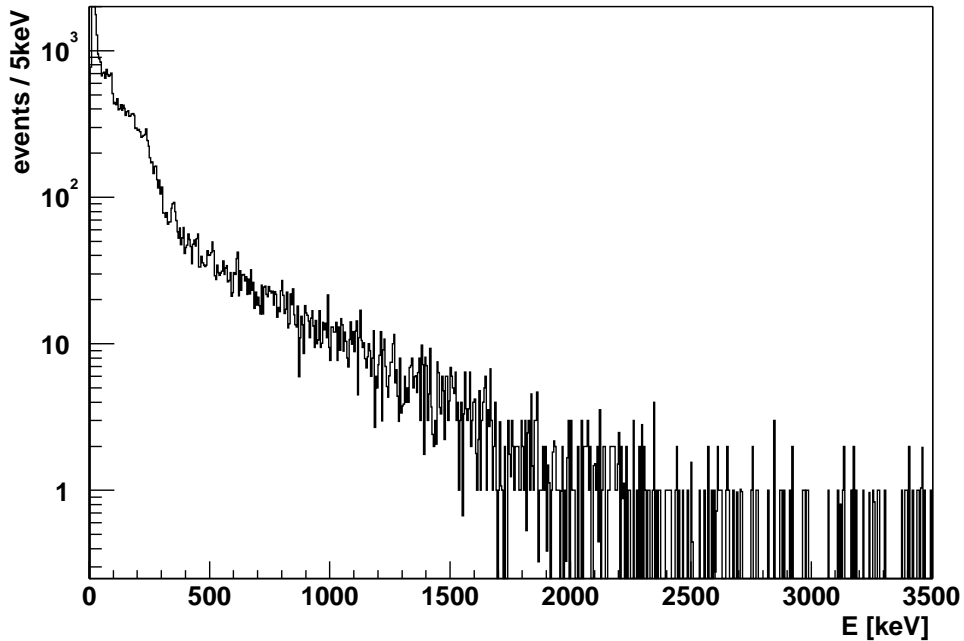


Fig. 6. Measured CPG spectrum up to 3.5 MeV for 134.5 g·d in events per 5 keV. Small peaks of the 351 keV and 609 keV lines of the ^{238}U decay chain can be seen. A shoulder at low energies due to the fourfold forbidden β -decay of ^{113}Cd is clearly visible.

1 MeV this effect does not show up, so that almost the full data set can be used, rejecting only burst runs with exceptional high count rates as for the CPG detector. The usable data set corresponds to 397.5 g·d.

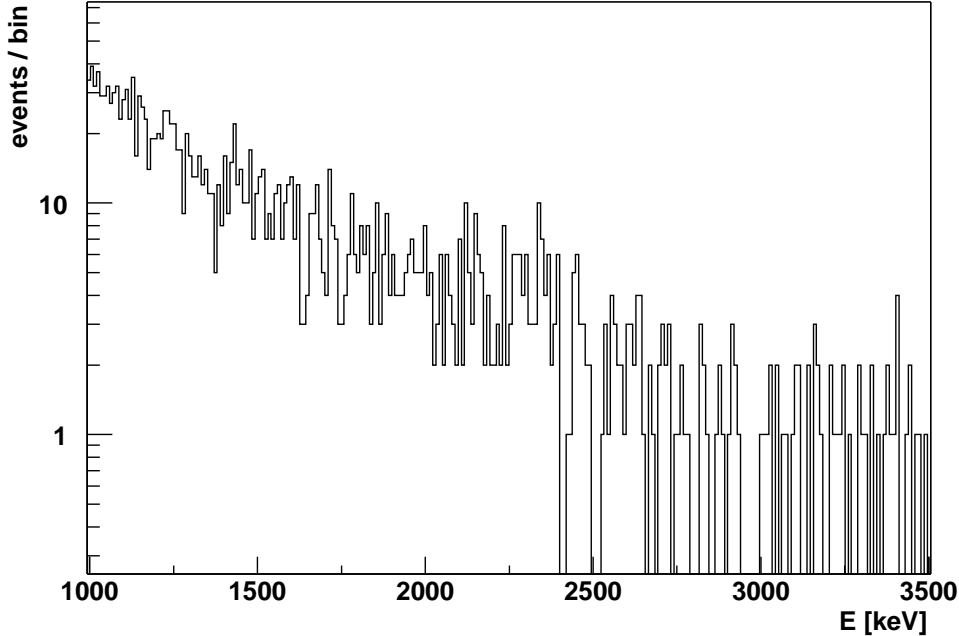


Fig. 7. Measured ER spectrum above 1 MeV in events per 9.45 keV. This spectrum corresponds to 397.5 g-d of data taking.

The spectrum recorded with the ER detector as shown in figure 7 does not reveal clear background lines mainly due to its worse energy resolution. Nevertheless, some ^{232}Th may be present implied by a slight enhancement of events around 2614 keV.

4 Data analysis

In case the half-life $T_{1/2}$ under investigation exceeds by far the measuring time ($t \ll T_{1/2}$) the radioactive decay law including the efficiency ϵ to detect the event is given by

$$T_{1/2} = \frac{N_0 \cdot \ln 2 \cdot t \cdot \epsilon}{n} \quad (12)$$

where N_0 is the number of atoms of a particular isotope in the source, t the time of measurement and n the number of observed events, or for limits the number of excluded events.

The efficiencies for both detectors have been calculated with the Monte Carlo package GEANT4 [19] and cross checked with the MCNP program package [20]. Both have been modified to generate double beta events via a neutrino mass term where the energy and angular distributions of the two electrons are simulated according to formulae given in [16]. All events are started homoge-

nously and isotropically in the whole detector. The simulations calculate the energy deposition of e^- , e^+ and γ from an event within the detector including Compton backscattering from the shielding. Both programs produce consistent efficiencies. As an example, the efficiencies for full absorption (resp. no energy deposition) of 511 keV annihilation gammas is 4.5% (85.0%) and 7.6% (79.2%) for the CPG and ER detectors. The efficiencies for no energy deposition of photons less than 1 MeV are shown in figure 8.

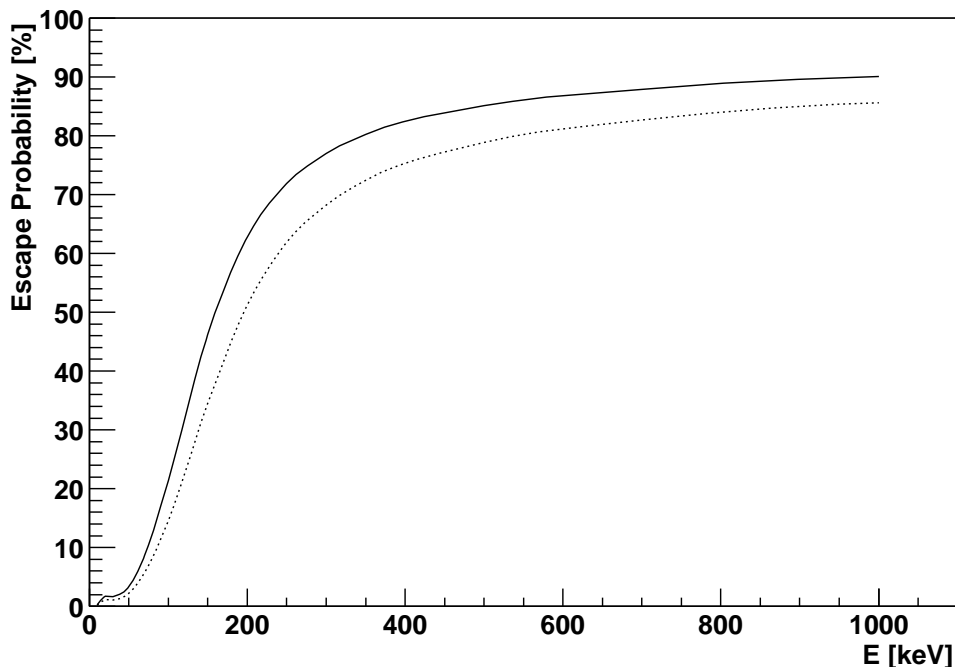


Fig. 8. Probability of a gamma to escape from a detector without energy deposition as a function of its energy as calculated with GEANT4. The solid line represents the CPG, the dotted line the ER detector.

The natural abundances, decay modes and Q -values of all isotopes under study are given in table 1. The composition of the CPG detector is given by $(\text{Cd}_{0.9}\text{Zn}_{0.1}\text{Te})$ with a density of 5.78 g/cm^3 . The density of the ER CdTe detector is 5.85 g/cm^3 .

In this analysis the lower limits of half-lives are obtained via the following χ^2 -method: The background around the position of the peak under investigation is fitted with an exponential function. A gaussian peak is then grown on the resulting function at the energy of the searched peak and with a width as described by the corresponding energy resolution of the detector. The $\chi^2(n)$ of this model function is calculated as a function of the number n of events in this peak, with which the null-hypothesis is checked. The obtained χ^2 can then be transformed into a function of the inverse half-life. To produce a joint limit for many spectra (in this case two) the $\chi^2((T_{1/2})^{-1})$ of the single detectors are added. The 90% CL lower limit can then be extracted by taking the half-life where $\chi_{sum}^2((T_{1/2})^{-1})$ is increased by 2.71 with respect to its minimum.

Isotope	decay mode	Q -value [keV]	nat. abund. [%]
^{64}Zn	$\beta^+/\text{EC}, \text{EC}/\text{EC}$	1096	48.6
^{70}Zn	$\beta^-\beta^-$	1001	0.6
^{106}Cd	$\beta^+\beta^+, \beta^+/\text{EC}, \text{EC}/\text{EC}$	2771	1.25
^{108}Cd	EC/EC	231	0.89
^{114}Cd	$\beta^-\beta^-$	534	28.72
^{116}Cd	$\beta^-\beta^-$	2805	7.47
^{120}Te	$\beta^+/\text{EC}, \text{EC}/\text{EC}$	1722	0.096
^{128}Te	$\beta^-\beta^-$	868	31.69
^{130}Te	$\beta^-\beta^-$	2529	33.80

Table 1

Decay modes, Q -values and natural abundances of isotopes under study.

5 Results

A variety of signatures of the different double beta decay modes are investigated. In all cases only neutrinoless modes are considered, except for double electron capture (EC/EC) where the neutrino accompanied mode is used.

The following limits are calculated according to the above χ^2 -method from 1117 h measurement with a 2.89 g CdZnTe detector (134.5 g·d) and additionally from 1645 h with a 5.8 g CdTe detector (397.5 g·d) for energies above 1 MeV.

5.1 $\beta^-\beta^-$ -transitions

The signal of the $0\nu\beta^-\beta^-$ -decay to the ground state of the daughter nucleus is a peak at the Q -value of the involved nuclear transition, which is given in table 1. Due to the fact that source and detector are identical the detection efficiency is high for this decay mode as can be seen from figure 9. Typical peak efficiencies assuming the neutrino mass mechanism are 55.5% (60.6%) for ^{116}Cd ($Q = 2.805$ MeV), increasing to 92.7% (94.0%) for ^{128}Te ($Q = 868$ keV) for the CPG (ER) detector. In case of right handed weak currents the efficiency of the CPG detector is slightly less, about 53%.

The isotope with the highest Q -value is ^{116}Cd . The background in the ^{116}Cd , where the exponential function is basically flat, can be estimated by averaging the spectrum from 2.7 to 3.4 MeV while excluding the peak region at 2.8 MeV to be $3.3 \times 10^{-4} [\text{keV}\cdot\text{g}\cdot\text{d}]^{-1}$.

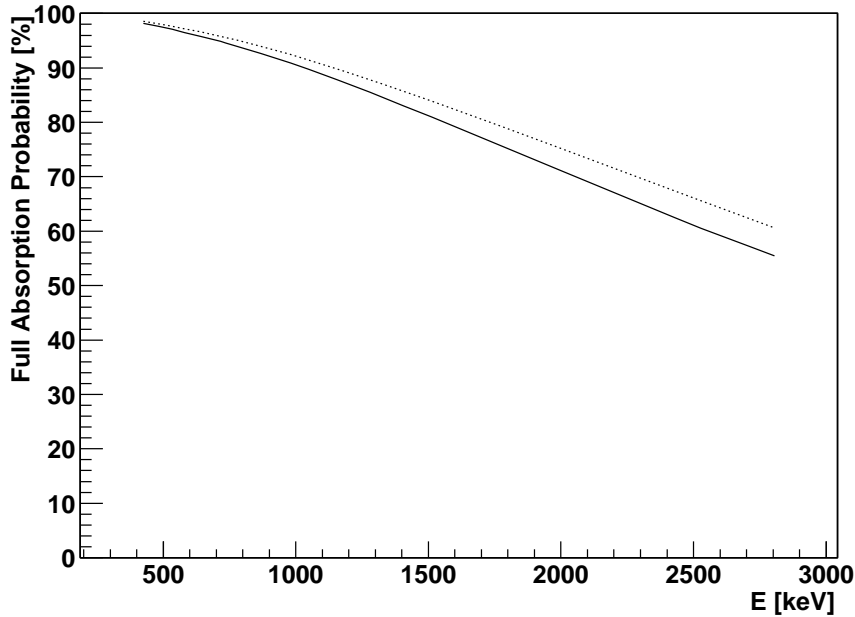


Fig. 9. Probability to detect the full energy of both electrons of a $0\nu\beta^-\beta^-$ -decay as calculated with GEANT4. The solid line represents the CPG, the dotted line the ER detector.

Figure 10 shows the region of interest for the CPG spectrum only. The dashed line represents the flat background plus a fitted ^{208}Tl line at 2614 keV of 6.4 ± 4.5 events. This background model yields a $\chi^2/\text{ndf} = 18.3/30$. The 90% CL excluded number of events for ^{116}Cd $0\nu\beta^-\beta^-$ -decay ($Q = 2805$ keV, 3.4 events) as obtained by the χ^2 -method is superimposed. In a similar fashion all other transitions are evaluated. Evidently, for ^{70}Zn (figure 11) only the CdZnTe detector (CPG) could be used. No peak is observed at any transition energy.

The search for transitions to excited states is also looking for a peak, however, at $Q - E_\gamma$, requiring that the energetic gammas of the de-excitation must leave the detector without any energy deposition through Compton scattering, photo effect or pair-production. De-excitation photons in the range from 400 keV up to 2.3 MeV are considered and are given in tables 2 and 3.

A typical escape efficiency for the ER detector is 86.1% for $E_\gamma = 1294$ keV (see figure 8) coming from the ^{116}Cd decay into the first excited state of ^{116}Sn (2^+). At all the relevant positions searches for peaks analogous to the ground state transitions were performed. A compilation of all obtained results is shown in table 2.

The achieved half-life limits are of the order of 0.7×10^{18} to 3.3×10^{19} yrs for various cadmium and tellurium $0\nu\beta^-\beta^-$ -modes. Using only a rather small amount of CdTe and CdZnTe it cannot be expected to probe the current

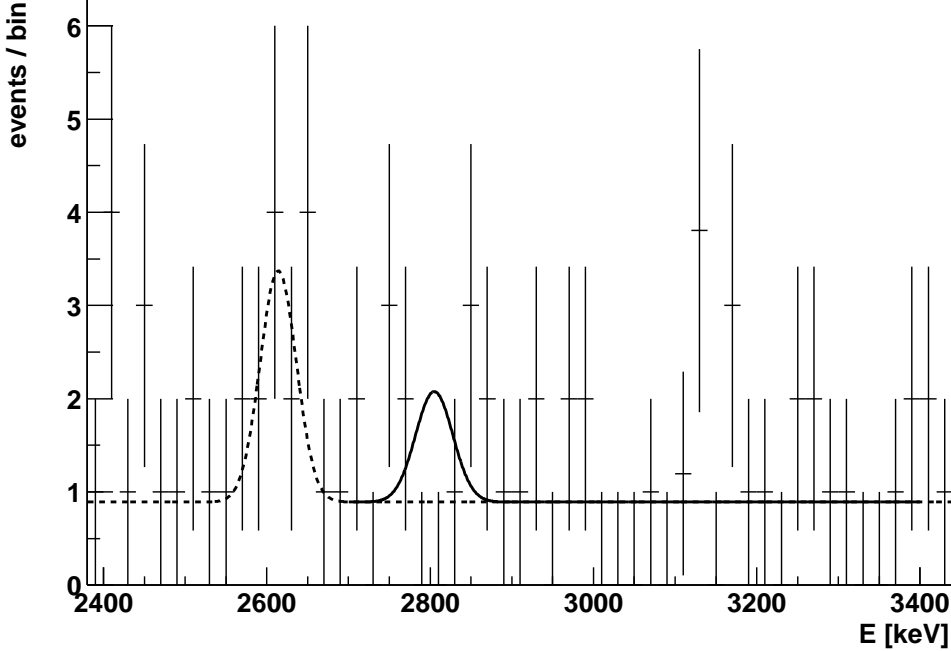


Fig. 10. Fit of constant background plus 2614 keV ^{208}Tl line (dashed line) with $\chi^2/\text{ndf} = 18.3/30$ and exclusion plot for 2805 keV ^{116}Cd $0\nu\beta^-\beta^-$ (solid line) using the rebinned CPG spectrum.

limits for ^{116}Cd and ^{130}Te [17]. Nevertheless, for ^{70}Zn an improved limit of $T_{1/2} > 1.3 \cdot 10^{16} \text{ yrs}$ (90% CL) is obtained.

5.2 $\beta^+\beta^+$ -transitions

The $\beta^+\beta^+$ -modes are more difficult to detect and have hence lower half-life limits. The energy available for the decay decreases by $2m_e c^2 = 1022 \text{ keV}$ per β^+ compared with the electron capture (EC) modes. The energy distribution of the positrons in a $0\nu\beta^+\beta^+$ -decay is the same as for the $0\nu\beta^-\beta^-$ -mode and the energy deposited by the two positrons is $E = Q - 4m_e c^2$. In the $0\nu\beta^+\text{EC}$ mode the total energy is carried away by the single positron only. Additionally, the energy of the electron capture process is added, again leading to a line at $E = Q - 2m_e c^2 + E_K$, because electron capture is dominantly from the K-shell. $2\nu\text{EC}/\text{EC}$ is only detectable via “soft” x-ray cascades or Auger electrons with a total energy of about two times the binding energy of the K-shell, assuming that K-capture is the major contribution to EC. Both possibilities can be detected equally well, because all the energy will be deposited in the CdTe detector. The EC/EC detection requires a rather low energy threshold. Only the CPG detector was used for that, running with a threshold of about 20 keV.

In previous searches mostly 511 keV annihilation gammas from the positrons were detected by external detectors. In our case also the positron energy can

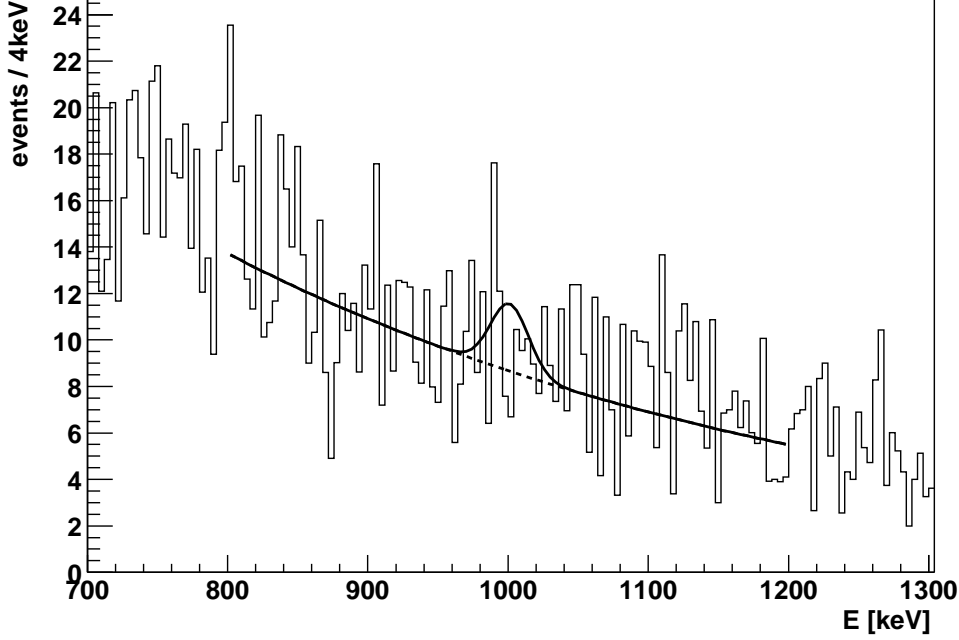


Fig. 11. Fit of exponential background (dashed line) from 800-1200 keV with $\chi^2/\text{ndf} = 213.8/99$ and exclusion plot for 1001 keV $^{70}\text{Zn } 0\nu\beta^-\beta^-$ (solid line) using the rebinned CPG spectrum. Using different fit intervals (750-1250, 800-1200 and 850-1250 keV), the number of excluded events is stable within 4%.

be measured to discriminate different isotopes. EC/EC can be investigated as well.

Like in the $\beta^-\beta^-$ -case, also here searches for excited state transitions can be performed. For the $0\nu\beta^+\beta^+$ and $0\nu\beta^+\text{EC}$ decays to excited states a line is searched at $E = Q - 4m_e c^2 - E_\gamma$ and $E = Q - 2m_e c^2 + E_K - E_\gamma$ respectively.

However, to distinguish EC/EC excited modes from the decay to the ground state, also the gamma has to be detected. Unfortunately, the efficiency to fully detect these gammas is quite poor (1.0% for $E_\gamma = 1171$ keV with the CPG detector, see figure 8), resulting in even lower half-lives. Therefore, for an upper limit it is more efficient to consider the more likely case that the de-excitation gamma escapes undetected (90.8% for $E_\gamma = 1171$ keV with the CPG detector) and apply this efficiency to the limit for the decay to the ground state.

Figure 12 depicts the exclusion plot for the $0\nu\beta^+\text{EC}$ decay of ^{120}Te . Having a Q -value of 1722 keV and a K-shell binding energy of about 30 keV, a peak is searched at $E = Q - 2m_e c^2 + E_K = 730$ keV. The dashed line shows the fitted exponential background with $\chi^2/\text{ndf} = 79.0/87$. The solid line shows the 90% CL excluded gaussian distribution. The same plot is shown in figure 13 for the $2\nu\text{ECEC}$ -process where the signal is expected at 2×30 keV=60 keV. The corresponding energies for ^{64}Zn and $^{106}\text{Cd}/^{108}\text{Cd}$ are 17 keV and 49 keV respectively.

Isotope	Level [keV]	$T_{1/2}$ [<i>yr</i> s]	existing limit on $T_{1/2}$ [<i>yr</i> s]
^{116}Cd	(0 ⁺) g.s.	8.0×10^{18}	7.0×10^{22} (90% CL)[21]
	(2 ₁ ⁺) 1294	1.6×10^{18}	1.3×10^{22} (90% CL)[21]
	(0 ₁ ⁺) 1757	2.7×10^{18}	7.0×10^{21} (90% CL)[21]
	(0 ₂ ⁺) 2027	7.0×10^{17}	2.1×10^{21} (90% CL)[22]
	(2 ₂ ⁺) 2112	1.6×10^{18}	1.7×10^{20} (68% CL)[23]
	(2 ₃ ⁺) 2225	7.1×10^{17}	1.0×10^{20} (68% CL)[23]
^{114}Cd	(0 ⁺) g.s.	6.4×10^{18}	2.0×10^{20} (90% CL)[24]
^{130}Te	(0 ⁺) g.s.	3.3×10^{19}	2.1×10^{23} (90% CL)[25]
	(2 ₁ ⁺) 536	1.8×10^{19}	9.7×10^{22} (90% CL)[26]
	(2 ₂ ⁺) 1121	1.4×10^{19}	2.7×10^{21} (90% CL)[27] (0+2 ν)
	(0 ₁ ⁺) 1794	3.1×10^{18}	2.3×10^{21} (90% CL)[27] (0+2 ν)
^{128}Te	(0 ⁺) g.s.	8.8×10^{18}	8.6×10^{22} (90% CL)[26]
	(2 ₁ ⁺) 443	1.3×10^{18}	4.7×10^{21} (68% CL)[28]
^{70}Zn	(0 ⁺) g.s.	1.3×10^{16}	4.8×10^{14} [29]

Table 2

Obtained lower limits (90% CL) on half-lives for $0\nu\beta^-\beta^-$ -decay modes to ground state (g.s) and excited states compared with existing limits. The limit for ^{70}Zn could be improved by more than an order of magnitude.

A compilation of all obtained limits is shown in table 3. For the various $\beta^+\beta^+$ -modes the limits are a few orders of magnitude lower than for $\beta^-\beta^-$ -decay, from 8.5×10^{15} to 1.0×10^{18} *yr*s. Some decays are investigated for the first time. Especially for various decay modes of ^{120}Te and $2\nu\text{ECEC}$ ground state transitions of ^{106}Cd , ^{108}Cd and ^{64}Zn new limits could be set.

6 Summary

The main intention of the paper is to show the reliability of CdTe detectors for the search of rare nuclear decays, especially double beta decay. Within the context of background studies for the planned COBRA-experiment [13], a setup consisting of two CdTe/CdZnTe detectors in a shielding was used to investigate various double beta decay modes of Cd, Te and Zn isotopes. The searches took advantage of the fact that source and detector are identical and of the good energy resolution of semiconductor detectors. With a collected statistics of 0.53 kg·d for energies beyond 1 MeV and 0.13 kg·d for energies below 1 MeV, limits of the order of 10^{19} *yr*s for various $0\nu\beta^-\beta^-$ -modes could be

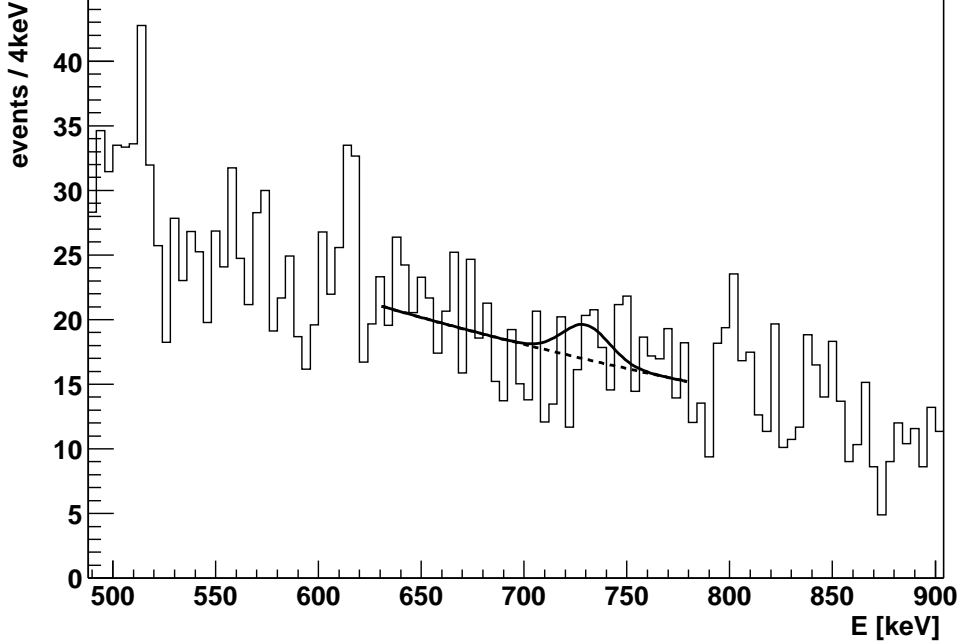


Fig. 12. Fit of exponential background (dashed line) from 630-780 keV with $\chi^2/\text{ndf} = 24.6/36$ and exclusion plot for 730 keV ^{120}Te $0\nu\beta^+\text{EC}$ (solid line) using the rebinned CPG spectrum.

obtained. A new improved limit for the $0\nu\beta\beta$ -decay of ^{70}Zn is given, which has not been investigated experimentally in the last fifty years. A detailed study of all available $\beta^+\beta^+$ -channels is performed, where for the first time values for the $2\nu\text{ECEC}$ -decay of ^{120}Te are obtained. Limits on the $0\nu\beta^+\text{EC}$ of ^{120}Te and the $2\nu\text{ECEC}$ for ground state transitions of ^{106}Cd , ^{108}Cd and ^{64}Zn were improved significantly.

Having shown with the obtained results, that CdTe can be used for low-level applications, because the material seems to be clean enough that an upgrade to larger detector masses like 10 kg as proposed in [13] would allow to probe neutrino masses below 1 eV. Especially in case of ^{116}Cd it seems to be possible to make the experiment background free. The main advantage is, that the half-life sensitivity scales with $M^{1/2}$ instead of $M^{1/4}$ as in the background limited case [15]. The first advantage is the high Q-value of 2805 keV of ^{116}Cd $0\nu\beta\beta$ -decay which is above all gamma-lines occurring in the natural decay chains. Thus this normally dominating background component can be neglected. The only beta decay in the natural decay chains with an endpoint higher than 2805 keV stems from ^{214}Bi , but this potential background can be easily vetoed because it is associated with the emission of a 7.68 MeV α -particle 164 μs later. The main remaining background expected are neutrons, especially because of the large cross section for neutron capture on ^{113}Cd , producing gammas up to 8 MeV. However, a severe neutron shield or an isotopical derichment of ^{113}Cd reduces the background significantly. Another background source is possible radio-isotopes produced by cosmic ray spallation. They were measured for the γ -astronomy mission INTEGRAL in a proton test beam at CERN [36] and

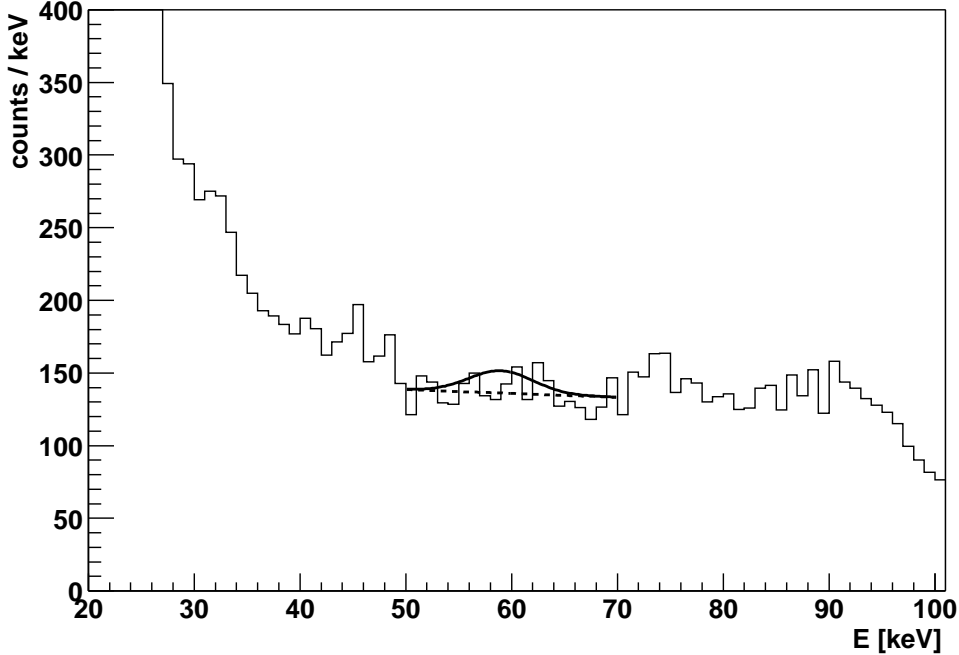


Fig. 13. Fit of exponential background (dashed line) from 50-70 keV with $\chi^2/\text{ndf} = 17.1/18$ and exclusion plot for a line at 59 keV from ^{120}Te $2\nu\text{ECEC}$ (solid line) using the rebinned CPG spectrum. The peaks of the $2\nu\text{ECEC}$ transitions of ^{64}Zn and $^{106}\text{Cd}/^{108}\text{Cd}$ lie at 17 keV and 49 keV respectively.

only two dangerous isotopes are identified. Fortunately they are all rather short-living and have a low branching ratio.

Last but not least, the tail of $2\nu\beta\beta$ -decay leaks into the peak region of $0\nu\beta\beta$ -decay, because it occurs with an orders of magnitude higher rate. The crucial quantity to keep this under control is the energy resolution of the detector. A very promising choice is a semiconductor like CdTe. For a To improve the neutrino mass further the experiment has to be upgraded to larger masses, which according to the modular design can be performed rather easily.

7 Acknowledgements

We thank C. Gößling for useful discussions and his support. We also acknowledge the support of Th. Villett and the mechanical workshop of the University of Dortmund during construction of the test setup. K. Zuber is supported by a Heisenberg Fellowship of the Deutsche Forschungsgemeinschaft. Finally we want to thank eV-PRODUCTS for lending a detector for test measurements.

Isotope	Level [keV]	Mode	$T_{1/2}$ [yrs]	existing limit on $T_{1/2}$ [yrs]
^{120}Te	(0 ⁺) g.s.	$0\nu\beta^+\text{EC}$	2.2×10^{16}	4.2×10^{12} [29]
	(0 ⁺) g.s.	$2\nu\text{ECEC}$	9.4×10^{15}	—
	(2 ₁ ⁺) 1171	$2\nu\text{ECEC}$	8.4×10^{15}	—
$^{106,108}\text{Cd}$	(0 ⁺) g.s.	$2\nu\text{ECEC}$	1.0×10^{18}	1.5×10^{17} (68% CL)[30] (g.s.+512)
^{106}Cd	(2 ₁ ⁺) 512	$2\nu\text{ECEC}$	8.3×10^{17}	3.5×10^{18} (90% CL)[31] (0+2 ν)
	(0 ⁺) g.s.	$0\nu\beta^+\beta^+$	1.5×10^{17}	2.2×10^{19} (90% CL)[32]
	(2 ₁ ⁺) 512	$0\nu\beta^+\beta^+$	7.4×10^{16}	1.6×10^{20} (90% CL)[33] (0+2 ν)
	(0 ⁺) g.s.	$0\nu\beta^+\text{EC}$	3.8×10^{17}	3.7×10^{20} (90% CL)[33]
	(2 ₁ ⁺) 512	$0\nu\beta^+\text{EC}$	2.2×10^{17}	2.6×10^{20} (90% CL)[33] (0+2 ν)
	(2 ₂ ⁺) 1128			
	+(0 ₁ ⁺) 1134	$0\nu\beta^+\text{EC}$	7.5×10^{16}	—
^{64}Zn	(0 ⁺) g.s.	$2\nu\text{ECEC}$	6.0×10^{16}	8.0×10^{15} [34]
	(0 ⁺) g.s.	$0\nu\beta^+\text{EC}$	2.8×10^{16}	2.3×10^{18} (68% CL)[35]

Table 3

Lower limits (90% CL) for $0\nu\beta^+\beta^+$, $0\nu\beta^+\text{EC}$ and $2\nu\text{ECEC}$ -decay to ground state (g.s) and excited states obtained from the COBRA test measurements compared with existing limits. For the transitions of ^{106}Cd to 1128 keV (2₂⁺) and 1134 keV (0₁⁺) only a joint limit can be given because of the finite energy resolution.

References

- [1] K. Zuber, Phys. Rep. 305 (6) (1998) 295.
- [2] M. Gell-Mann, P. Ramond, R. Slansky, Proceedings Supergravity (1978) 315.
- [3] T. Yanagida, Prog. Theor. Phys. B 135 (1978) 66.
- [4] R. N. Mohapatra, G. Senjanovic, Phys. Rev. Lett. 44 (1980) 912.
- [5] K. Zuber, Prog. Part. Nucl. Phys. 48 (2002) 223.
- [6] M. Doi, T. Kotani, E. Takasugi, Prog. Theor. Phys. Suppl. 83 (1985) 1.
- [7] R. Mohapatra, Phys. Rev. D 34 (1986) 3457.
- [8] M. Hirsch, H. Klapdor-Kleingrothaus, S. Kovalenko, Phys. Lett. B 352 (1995) 1.
- [9] M. Doi, T. Kotani, Prog. Theor. Phys. 89 (1) (1993) 1139.
- [10] M. Hirsch, et al., Zeit. f. Physik A 347 (1994) 151.
- [11] H. Klapdor-Kleingrothaus, et al., Mod. Phys. Lett. A. 16 (2002) 2409.

- [12] C. Aalseth, et al., *Mod. Phys. Lett. A.* 17 (2002) 1475.
- [13] K. Zuber, *Phys. Lett.B* 519 (2001) 1.
- [14] C. Lederer, V. Shirley, *Table of Isotopes*, 7th Edition, John Wiley and Sons, New York, 1978.
- [15] S. Elliott, P. Vogel, *Ann. Rev. Nucl. Part. Sci.* 52 (2002) 115.
- [16] V. Tretyak, Y. Zdesenko, *Atomic Data and Nuclear Data Tables* 61 (1995) 43.
- [17] V. Tretyak, Y. Zdesenko, *Atomic Data and Nuclear Data Tables* 80 (2002) 83.
- [18] M. Amman, P. Luke, *IEEE Trans. Nucl. Sci.* 46 (3) (1999) 205.
- [19] K. Amako, *Nucl. Instrum. Methods Phys. Res., A* 453 (2000) 455.
- [20] J. Briesmeister, Los Alamos National Laboratory LA-13709-M.
- [21] F. Danevich, et al., *Phys. Rev. C* 62 (2000) 045501.
- [22] A. Piepke, et al., *Nucl. Phys. A* 577 (1994) 510.
- [23] A. Barabash, A. Kopylov, V. Cherehovskiy, *Phys. Lett. B* 249 (1990) 186.
- [24] A. Georgadze, et al., *Physics of Atomic Nuclei* 58 (7) (1995) 1093.
- [25] C. Arnaboldi, et al., hep-ex/0211071 .
- [26] A. Alessandrello, et al., *Phys. Lett. B* 486 (2000) 13.
- [27] A. Barabash, et al., *Eur. Phys. J. A* 11 (2001) 143.
- [28] E. Bellotti, et al., *Europhys. Lett.* 3 (8) (1987) 889.
- [29] J. Fremlin, M. Walters, *Proc. Phys. Soc. A* 65 (1952) 911.
- [30] E. Norman, M. De Faccio, *Phys. Lett. B* 148 (1984) 31.
- [31] A. Barabash, et al., *Nucl. Phys. A* 604 (1996) 115.
- [32] F. Danevich, et al., *Z. Phys. A* 355 (1996) 433.
- [33] P. Belli, et al., *Astropart. Phys.* 10 (1999) 115.
- [34] A. Berthelot, et al., *Compt. Rend.* 236 (1953) 1769.
- [35] E. Norman, *Phys. Rev. C* 31 (1985) 1937.
- [36] E. Porras, et al., *Nucl. Inst. Meth. B* 111 (1996) 325.